Sensors and Materials, Vol. 18, No. 4 (2006) 183–197
MYU Tokyo

S & M 0642

Developing Miniature Nanostructured Semiconductor-Metal-Oxide Gas Sensors

Jian-Wei Gong and Quan-Fang Chen*

MEMS and Nanomaterials Laboratory,
Department of Mechanical, Materials and Aerospace Engineering, University of Central Florida,
Orlando, FL, 32826, U.S.A.

(Received April 21, 2005: accepted November 8, 2005)

Key words: MEMS sensor, nanostructured SMO, ambient temperature, relative humidity, feedback control

Micromachined nanostructured semiconductor-metal-oxide (SMO) gas sensors have proven promising in gas detection due to their improved sensitivity, robustness, simple signal processing, low fabrication cost and low energy consumption. However, the development of nanostructured micro-SMO sensors must not only satisfy performance-related requirements, but also face reliability-related challenges, particularly false alarm problems caused by environmentally induced drift and shift. In this article, we present results obtained in the development of a novel nanostructured micromachined SMO gas sensor and discuss the challenges in finding solutions to minimize the influences of environmental factors such as temperature, relative humidity, light and oxygen partial pressure.

1. Introduction

Semiconductor sensors have become one of the major players in gas detection since they were first reported by Brattain and Bardeen in 1952.[1] Taguchi developed semiconductor-metal-oxide (SMO) gas sensors as commercial products in the 1960s.[2–4] Most current commercially available semiconductor sensors are manufactured by screen-printing techniques on small, thin ceramic substrates.[5,6] N-type SMOs like SnO_2, ZnO, TiO_2 and WO_3 are commonly used as gas sensing materials, while SnO_2 is by far the most widely used oxide. The gas detection principle of semiconductor gas sensors is based on variations of the depletion layer at the boundaries in the presence of reducing or oxidizing gases. The variations in the depletion layer reflect the height changes of the energy barriers for free charge carriers (e.g., electrons in SnO_2).[7,8] Reducing gases lower the energy barrier while oxidizing gases increase it. The extent of the change has been successfully used as the detected signal (e.g., resistance). These SMO sensors are best suited for

*Corresponding author, e-mail address: qchen@mail.ucf.edu

detecting harmful gases such as CO, H_2, H_2S, NO_x and hydrocarbons (propane, butane, etc.) at low concentration levels, because of their high sensitivity, robustness, simple signal processing, low production cost, small size and low power consumption.

Generally speaking, the development of a commercially ready gas sensor must fulfill many requirements that are imposed by the intended application and the necessity to withstand various challenges encountered in the environment during the sensor's operation. The main requirements can be classified into two categories. The first includes performance-related issues such as sensitivity, selectivity, response time and recovery time. The second includes reliability-related issues such as drift, stability and interfering gases. Some concerns arise in the use of conventional SMO gas sensors in terms of cross-sensitivity, environmental influences including temperature and relative humidity, and power consumption.[9–12] Research has been focused on these and other aspects to develop better SMO sensors. For example, solutions for cross-sensitivity include but are not limited to the selection of dopants and/or catalysts on the basis of the scanning sensor working temperature, and the use of a sensor array together with a pattern recognition algorithm.[13–17] Nanocrystalline structured gas sensing materials have been developed to enhance the sensitivity of a SMO sensor[18] by increasing the surface-to-volume ratio. Ultrahigh-sensitivity SMO sensors have recently been developed and reported.[19–21] On the other hand, microelectromechanical systems (MEMS) and microfabrication technology have been used to reduce the gas sensor's power consumption to less than 100 mW, even at operation temperatures as high as 400°C.[22–24]

In this article, the authors introduce a series of newly developed gas sensors realized with a combination of nanostructured sensing film and microfabrication technology. Test results for hydrogen and hydrogen sulfide detection are presented. Environmental factors that affect the performance of SMO sensors, including temperature, relative humidity, light, and oxygen partial pressure, are discussed.

2. Materials and Methods

The gas sensing film is the key part of SMO gas sensors. Film fabrication methods can be categorized in three main groups: powder/slurry deposition, chemical vapor deposition (CVD), and physical vapor deposition (PVD). The main difference between powder/slurry-based films and CVD or PVD films has traditionally been their different film thicknesses. While the former yields sensitive layers several microns thick (thick films), the thickness of CVD or DVD layers varies between 20 and 1000 nm. However, it is necessary to point out here that spin-coating techniques, in which SMO slurry is used, can achieve 'thin films' (the slurry can be obtained by a sol-gel process) with controllable porosity. The sol gel process is a very promising technology for fabricating nanostructured thin films for sensing gases. Advantages compared with conventional vapor processing techniques include simple equipment with the possibility of low-temperature fabrication, the ability to produce ultrafine particles, the ability to control the sample shape, and the addition of multiple dopants simultaneously and accurately. High porosity and large surface area enhance sensitivity. The preparation of sols using either alkoxide or chloride precursors utilizing either dip- or spin-coating methods has been reported.

The SMO solution or sol is the key part of porous nanocrystalline layer development. A precursor (25 ml) of tin isopropoxide ($Sn(O^iPr)_4$, 10%, Alfa Aesar) and 5 ml deionized water were first mixed into 50 ml anhydrous ethanol, followed by magnetic stirring for 30 min. Then a complexing agent, acetylacetone (AcAc, 3 ml) was added to stabilize the hydrolysis of tin isopropoxide. After complete mixing by magnetic stirring for 2 h, a 10 wt% triblock copolymer, Pluronic F127 (PEO-PPO-PEO), was dissolved into the solution.[19,20] This solution was put on a hot plate at 50°C and stirred for two days. The viscosity of the sol was adjusted by adding polyvinyl alcohol (PVA). The resultant sol was filtered 7 times before use.

A nanostructured SnO_2 thin film was fabricated by spin coating the sol and subsequently calcining it. A ramp spin-coating method was used in which the spinning speed was gradually increased to 5,000 revolutions per minute (rpm) and then maintained at that speed for 30 s in total. After air drying for 1 min, the film was spin coated and air dried repeatedly when multiple coatings were needed to increase the thickness. The coated film was dried in an oven at 100°C for 30 min. The film was calcined in a furnace (Thermolyne) at a heating rate of 2°C/min to 500°C; this temperature was then maintained for 2 h. The thickness of SnO_2 film was measured with a Tencor® Profile Meter. The measured thickness was approximately 150 nm for a single spin coating at 5000 rpm.

The sol-gel method allows easy manipulation for adding doping material to achieve selectivity with atomic-level mixing and uniform dispersion efficiency. For the detection of H_2 and H_2S, Ag and Pt were added as doping material to SnO_2 to achieve better sensitivity and selectivity during this study. For Ag doping, $AgNO_3$ was added to the SnO_2 solution followed by magnetic stirring (for 24 h), while HNO_3 was used to stabilize the SnO_2 solution. Pt metal was introduced as a catalyst by sputtering. After the SnO_2 thin film was spin coated and calcined, Pt was sputtered onto the surface of the film followed by a thermal diffusion process. Figure 1 shows an SEM image of a silver-doped tin dioxide film fabricated by the sol gel process and a sketch of the gas sensor developed. The white spots in the SEM image are areas of silver oxide.

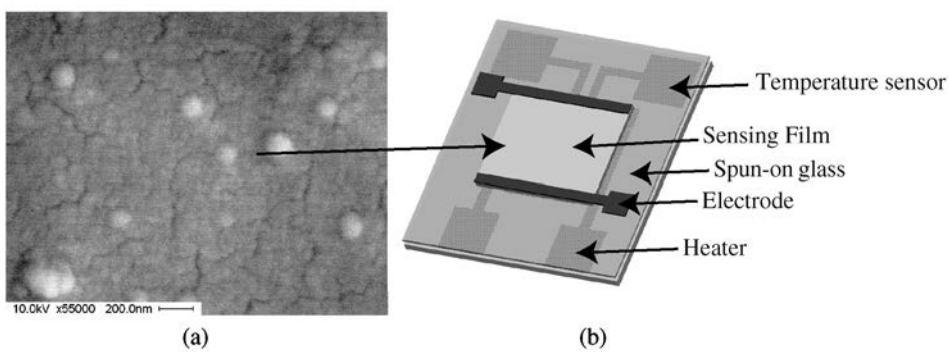

Fig. 1. (a) SEM image of an AG-doped SnO_2 film fabricated by the sol-gel process and (b) a sketch of the sensor layout.

The sensor sketched in Fig. 1(b) was fabricated by the micromachining method described elsewhere[25] and was tested in a calibrated chamber with predefined concentrations of hydrogen. The gas sensing properties of SnO_2 semiconductor thin films depend strongly on the method of fabrication. It has been pointed that crystallite size and film thickness have pronounced effects on gas sensitivity. SnO_2 semiconductor thin film can achieve maximum gas sensitivity only if the crystallite size within the film is comparable to the thickness of the space-charge layer (6 nm for SnO_2 at room temperature). Crystallite size also affects another important property of a semiconductor gas sensor, the surface-to-volume ratio. The smaller the particle size, the larger the surface-to-volume ratio (inversely proportional to the particle size). For example, a decrease in particle size from 100 μm to 20 nm increases the surface-to-volume ratio 5000 times. Hence a marked increment in sensitivity can be realized.

3. Results

The testing system consists of detected gas (H_2 or H_2S) cylinders and pure air gas cylinders with regulators (Airgas), a 2 cc/min mass flow controller (Omega), flowmeters, a gas chamber, and an oscilloscope (TDS 224) combined with the National Instrument Data Acquisition system. The chamber is first purged completely with pure air, and H_2 or H_2S gas is introduced into the chamber at the desired concentration by the mass flow controller. The concentration range of hydrogen is from 1000 ppm to 1% (10000 ppm). Then, pure air is introduced again for gas sensor recovery.

The fabricated sensors were tested as gas detectors. The results for a SnO_2+Pt thin film gas sensor and a SnO_2+Pt+Ag thin film gas sensor exposed to a series of hydrogen concentrations are presented in Fig. 2, and the gas sensing performances of these two

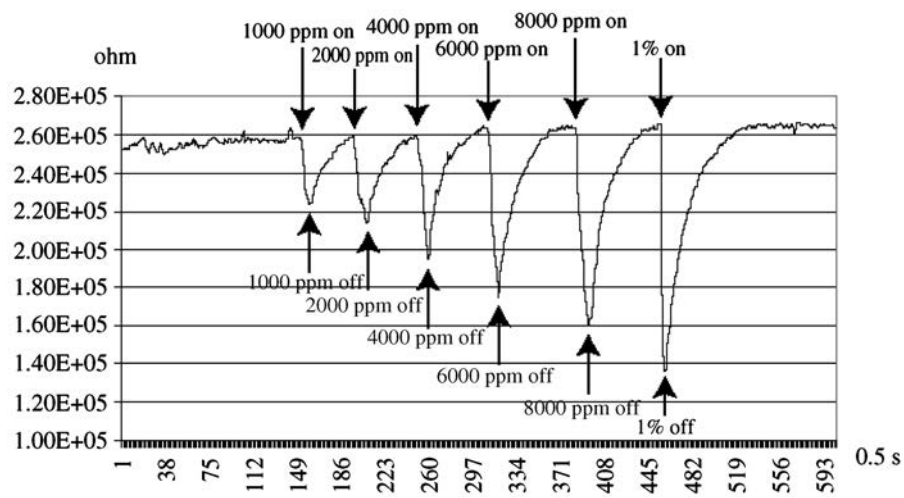

Fig. 2. Response of SnO_2+sputtered Pt H_2 at 250°C.

sensors is summarized in Table 1. The results show that the SnO_2/Pt/5%Ag film exhibits better sensing results than the SnO_2+Pt film. We observe that the SnO_2/Pt/5%Ag film has less baseline drift, better sensitivity, faster response time and quicker recovery time in comparison with SnO_2/Pt film. Doping with Ag improved the sensing ability of SnO_2 thin film to hydrogen. Another characteristic of both sensors is a fast response time (~2 s□predetermined from the long reaction time) and a quick recovery time (10–20 s).

The SnO_2 sensors doped with Ag were tested for H_2S detection. For better comprehension and comparison purposes, a Figaro (tin oxide) H_2S sensor (TGS825) was also tested. The results are summarized in Table 2.

Table 2 gives the sensitivity vs H_2S concentration for the two gas sensors tested. It is clear that our fabricated nanostructured sensor (UCF sensor) has better sensitivity than the Figaro sensor. Moreover, since the UCF sensor operates at a much lower temperature (74°C), the UCF sensor consumes less energy. The lowest concentration tested was 1 ppm.

4. Discussion

The thickness of the nanocrystalline SnO_2 thin film is an important factor that greatly affects its sensitivity to gases. Unlike TiO_2, which is a bulk conductance effect semiconductor, SnO_2 is a surface conductance effect semiconductor. The interaction between a semiconductor surface and H_2 or H_2S (with reducing properties) can be explained in terms of the reaction of hydrogen molecules with preadsorbed oxygen. Shukla and Seal[26] proposed that the sensitivity of a nanocrystalline SnO_2 thin film increases as the film thickness decreases. However, below a critical film thickness of ~110 nm, the gas sensitivity decreases with a further decrease of the film thickness. Very compact films exhibit lower surface areas and thus reduced Knudsen diffusion coefficients. As a result, they offer a reduced number of active sites for oxidation reactions with reducing gases, and hence the gas sensitivity is reduced as film thickness decreases below the critical thickness. In this investigation, the thickness of the nanocrystalline SnO_2 film is 100–150 nm. The nanofilm, fabricated using the polymeric sol-gel process together with a block copolymer structure-directing method, is mesoporous. Therefore, the number of active sites is increased significantly. The performance of the nanocrystalline SnO_2 sensor depends upon both the thickness and the mesoporous structure.

Table 1
Sensitivity to 250% hydrogen.

	1000 ppm	2000 ppm	4000 ppm	6000 ppm	8000 ppm	1%	Response time	Reaction time
SnO_2/Pt	18%	22%	30%	44%	63%	85%	~2 s	~20 s
SnO_2/5%Ag/Pt	30%	41%	53%	64%	79%	100%	~2 s	~10 s

Note: Sensitivity = $(R_1–R_0)/R_0\times100$, where R_1 is the resistance of the gas-sensing thin film in air, and R_0 represents resistance in gas environment of pure air.

Table 2
Sensitivity of H_2S detection.

	3 ppm	6 ppm	10 ppm	15ppm	20 ppm	25 ppm	50 ppm
Figaro	19%	54%	75%	82%	82%	82%	82%
UCF	40%	82%	92%	96%	97%	98%	99%

However, in addition to good functional performance, for practical applications, the sensor also must withstand various challenges encountered in the environment during sensor operation. These challenges include changes in temperature and humidity, as well as other potential effects that must be identified. These reliability-related concerns are more critical for sensor commercialization than the performance. If not appropriately accounted for, environmental influences such as ambient temperature and relative humidity become key influential factors in the instability of SMO sensors and the problem of false alarms. In most cases, sensor output contains a constant term as a reference (air) which is irrelevant to the detection of the target gas. For example, the sensitivity S is defined as $S_1 = (R_0–R_1)/R_0 \times 100$ or $S_2 = (R_0–R_1)/R_1$, where R_0 is the baseline resistance in air, and R_1 is the resistance in the environment of the gas to be detected. R_0 is assumed to be constant, but when the air shifts because of changes in the environmental conditions or drifts with time, the reliability of gas sensing is undermined. This is a serious issue, particularly when absolute values of target gas concentration are critical to safety concerns. Therefore, it is very important to understand quantitatively the shift in the air resistance of semiconductor gas sensors under the influence of environmental factors in order to diagnose or calibrate the sensors used in different applications.

4.1 *Ambient temperature effects*

Since changes in SMO sensor resistance caused by gas chemisorption are the mechanism for gas detection, any resistance variation due to environmental temperature changes will cause serious problems if not fully accounted for.

4.1.1 *Temperature-resistance relationship*

From the band-gap theory of semiconductors,[27] we know that a semiconductor's resistance is a function of temperature. The resistance is a nonlinear function of temperature that can be approximated by

$$R_T = R_0 e^{[\beta(1/T - 1/T_0)]},$$

where R_T and R_0 are the resistance values at absolute temperatures T and T_0 (on the Kelvin scale), respectively. β is a constant over a limited temperature range and is related to the material's properties.

4.1.2 *Ambient temperature effect as a superposition*

A fabricated SMO sensor is normally calibrated in-house at room temperature before being shipped out for service. The sensor's working power is normally fixed to maintain

the sensor's working temperature (for example, 250°C for our CO sensor) at the condition tested. However, experiments have been carried out specifically to address what happens if the environment temperature changes a few degrees, for example, from day to night.

The test results in Fig. 3 show that, when the ambient temperature changes from 27°C to 41°C (night to day in the summer in Florida), the working temperature of the device changes from 112°C to 125°C at constant power. The rise in ambient temperature adds to the sensor's working temperature under the same power. From eq. (1), we know that this temperature change induces a change in resistance that adds to the sensor's output, causing false signals if the device does not compensate for this effect.

4.1.3 *Schemes to eliminate temperature effects*

Published literature shows that efforts have been made to address the above issue, but studies have focused primarily on fabrication-induced instabilities. For example, Esch et al.[28] investigated the stability of Ti/Pt heater elements of the gas sensor influenced by diffusion and oxidation processes taking place during thermal treatments. However, the stability of a heater and its power does not mean that the gas sensor is unaffected by fluctuations in the ambient temperature. Our test results have shown that a fluctuation of a few degrees in ambient temperature adds to the working temperature of the device. As a result, this causes resistance changes in the gas sensor that compromise the chemical detection. To take this into account, Figaro's TGS sensor configuration[29] and some other designs[30] have external themistors to compensate for the induced temperature effect. This technique requires a fixed temperature-resistance relationship in the gas sensor. However, this is not guaranteed because of variations in the sensing material, during fabrication, and in the range of temperature change, as well as interactions with different gases that come into contact with the sensor. Commercial temperature stabilization circuits are available from Capteur,[31] in which the sensor heater forms part of a Wheatstone bridge. The current through the heater is controlled to maintain the sensor at a constant resistance. In other words, the heater is also used as the temperature sensor to simplify the design. However, the drawback of this scheme is that the temperature of the heater is not neccesarily the

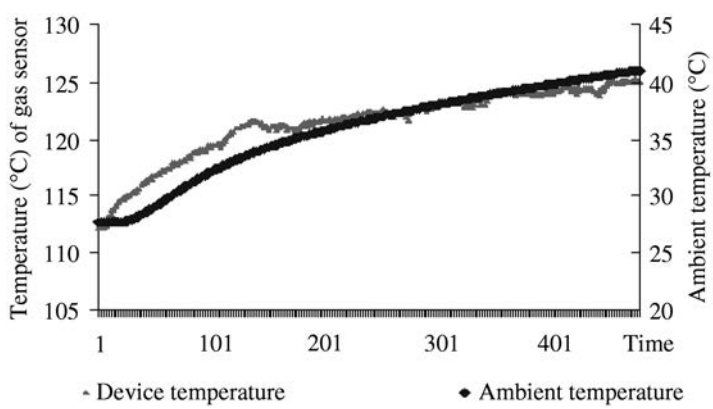

Fig. 3. Ambient temperature superimposed on temperature of sensors.

sensor's working temperature, particularly during the period of heating. For example, Pt has much better thermal efficiency than a ceramic substrate, which means the Pt heater (a small volume of material) can reach a required temperature much faster than the sensor's ceramic substrate. The heater's temperature must be higher than the required temperature (extra power must be provided) during temperature-compensation heating when the environment is cool. The extra heating current and the time depend on the environmental temperature and the mass of the sensor, as well as thermal convection (cooling). Therefore, it may be very difficult to achieve a thermal balance with this design. In summary, it is necessary to control and maintain the working temperature of the gas sensor at a constant level. The detection by the noise induced in the environmental temperature can thus be prevented.

The authors have developed a new temperature feedback control method to eliminate the influence of ambient temperature on the MEMS SMO gas sensor.[32] The sensor uses a separate built-in Pt resistor as a temperature sensor and heater to monitor and maintain the working temperature of the gas sensor at a constant value. The Pt resistance is linear with temperature over a wide temperature range. The sensor temperature changes as the ambient temperature changes, particularly for a MEMS-based sensor for which the volume is small, when the heating power remains constant. If the change in the Pt resistance of the temperature sensor can be measured precisely, this resistance change can be converted into the temperature change of the sensor substrate. Temperature floating can be adopted as a means of feedback control to maintain a constant sensor temperature by controlling the current to the heater. A separate Pt temperature sensor can monitor the heating power until the required working temperature is attained. As a result, the gas sensor's working temperature is automatically controlled with respect to the fluctuation of the ambient temperature, and a predefined working temperature may be constantly maintained. This eliminates the drift problem in the SMO gas sensor's baseline resistance caused by ambient temperature variation. Therefore, the possibility of false alarms is reduced or completely eliminated. Unlike indirect resistance compensation or software adjustments, the feedback control circuit described in this paper achieves real-time, large gain feedback.

The experimental results (Fig. 4) show improved gas sensor baseline stability and measurement precision. Figure 4 shows the data for sensors with and without feedback temperature control under the same environmental conditions. The resistance of the sensor with feedback temperature control only drifted within about 5 percent of its baseline resistance, while the resistance of the sensor without temperature control dropped more than 40% (Fig. 4). This 40% resistance change means that large false signals would result.

4.2 *Influence of humidity*

Relative humidity is another major concern regarding reliability-related requirements of the SMO sensor. It is well known that water vapor strongly influences the sensor's conductance G both in air and in air containing a reducing gas.[33–35]

4.2.1 *Influence of humidity on baseline resistance*

Madou and Morrison noted that the lower the humidity, in general, the greater the dependence of SMO sensors on relative humidity (RH).[36] When humidified air was introduced in a background of synthetic air, resistance decreased rapidly as the humidity

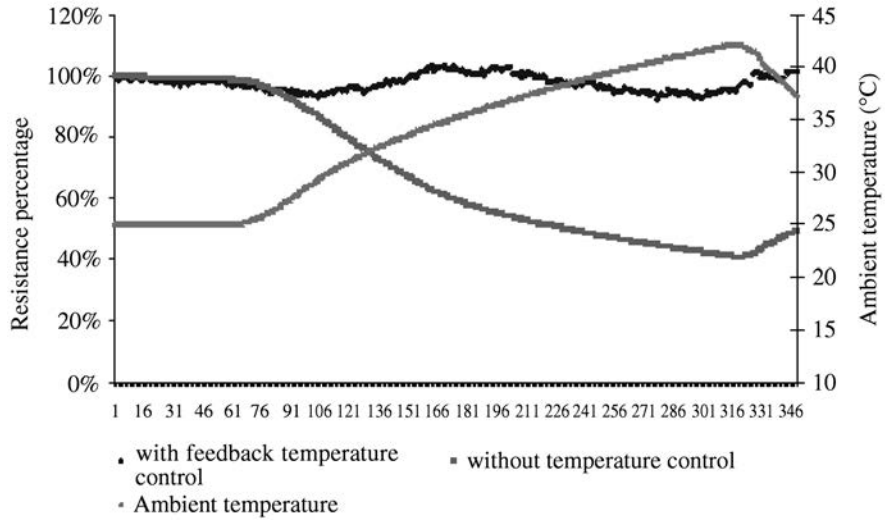

Fig. 4. Gas sensor behavior with varying ambient temperature.

increased. The momentum slows down as the humidity increases further until a constant resistance is reached. These dynamic responses have already been described for SnO_2, In_2O_3, ZnO and WO_3.[37–40] The decrease in resistance with increasing humidity was attributed to the dissociative reaction of water with oxygen in the lattice, which leads to the formation of oxygen vacancies and thus to a decrease in resistance. The change in resistance may be slow because of the recombination of OH ions with the oxygen vacancies in the lattice formed previously. Our test results (Fig. 5) for two SMO sensors (an original UCF SnO_2 sensor and a commercial Bacharach WO_3 sensor from Scott Instruments) also show these trends: the baseline resistance of the gas sensor decreases when RH increases. In the range where RH is lower than 30%, the curve is steeper, whereas in the range where RH is higher than 30%, the curve is more moderate.

This phenomenon can be explained as a sequence of dissociations and reductions. A hydrogenation reaction of absorbed water may involve a proton from a water molecule. A proton from a water molecule (a strong Brønsted acid) is more easily available than a tightly bound proton from an OH group (weak Brønsted acid).[41] Therefore, the process described in eq. (2) takes place, and the oxygen vacancy on the right-hand side of the equation must move towards the bulk in order to become effective as a donor.

$$H_2O + Sn + O \rightarrow 2(OH - Sn) + V_O \tag{2}$$

4.2.2 *Influence of humidity on sensor sensitivity*

Yannopoulos[42] claimed that the sensor device was relatively insensitive to humidity in the humidity range from 20% RH to 100% RH, although sensor resistance decreases when RH is above 70% because of instability caused by water condensation. A model for the interaction between CO and the SnO_2 surface, which takes into account the role of water vapor, was proposed by Bârsan and Ionescu.[43] They referred to the interaction of water

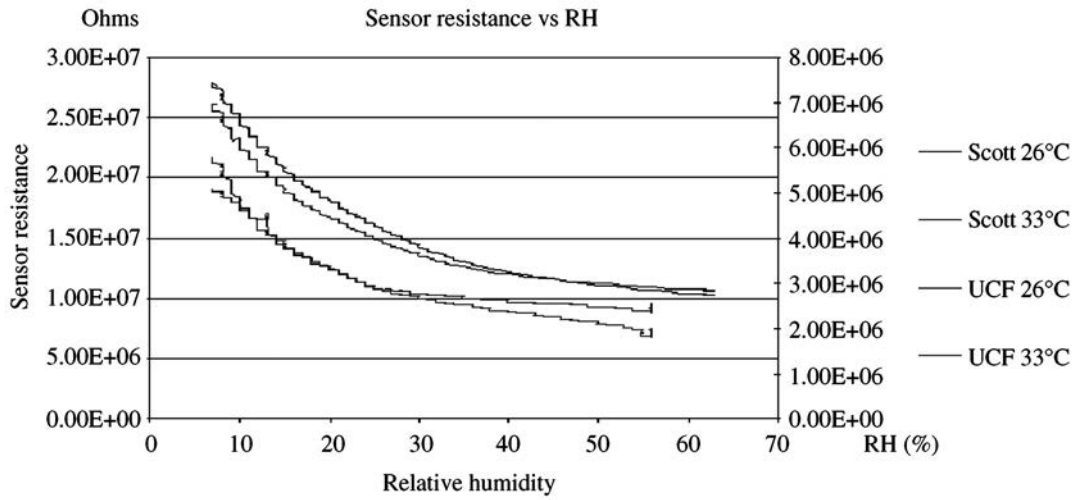

Fig. 5. Effect of relative humidity on gas sensor baseline resistance.

vapor with the SnO_2 surface as a process that generates chemisorption sites for oxygen and concluded that the reacting chemisorbed species of oxygen is a doubly ionized oxygen atom and that its interaction with reducing gases is enhanced by the presence of water vapor.

However, our test results show that the sensitivity of the SnO_2-H_2S sensor is greatly affected by relative humidity, even at levels higher than 30%. Tests were conducted on two SMO sensors, namely, the UCF SnO_2 sensor and the Bacharach WO_3 sensor, over a full range of H_2S concentrations (1 ppm–25 ppm) in different RHs (7%–98%). Figure 6 shows one results, i.e., 5 ppm H_2S test at different RHs. Summaries of repeated results are plotted in Fig. 7 to show the trend of the RH effect on sensor sensitivity.

From Fig. 7 it is clear that the sensor sensitivity decreases as the relative humidity increases for the same concentration of H_2S in air. We conclude that water molecules probably compete with H_2S molecules and prevent oxygen ions from reacting with H_2S. When dry air is reintroduced, the previous sensor resistance is recovered. The recovery time depends on the desorption of adsorbed H_2S molecules.

4.2.3 *Schemes to cope with humidity effects*

Many techniques have been proposed to deal with the problem of the influence of relative humidity. One method is to incorporate additives such as tin oxide into the sensing material. However, with this method, it is impossible to eliminate the influence of water to an acceptable level.[36] Another method is to use an array of sensors to convert the response of the sensor array using mathematical algorithms to obtain a response that is insensitive to water vapor.[44] Geloven et al.[45] use a method of switching a single tin oxide gas sensor between two well-defined temperatures to decrease the sensitivity to water vapor to an acceptable level. Huyberechts et al.[46] proposed the use of a combination of two metal-oxide-based sensors and a humidity sensor to form a microsystem with a trained artificial neural network. Another method includes compensation of the moisture effect by referring

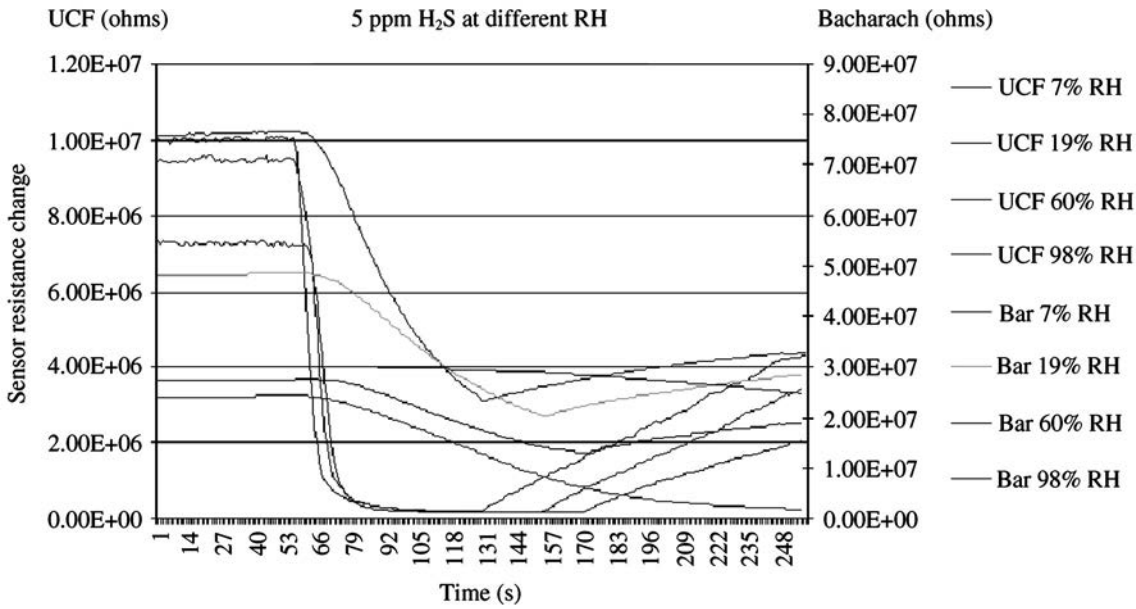

Fig. 6. 5 ppm H_2S test at different RH.

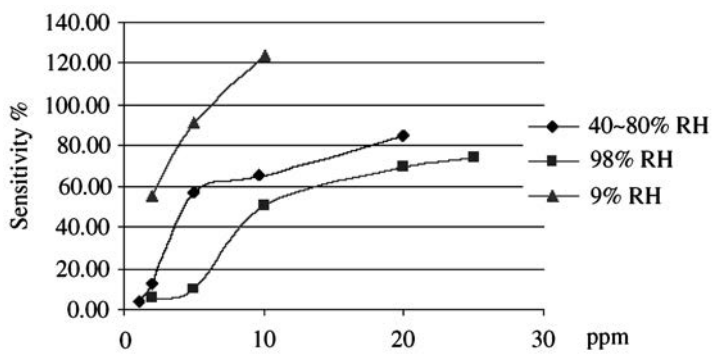

Fig. 7. RH effects on H_2S sensitivity.

to a compensation device, which is exactly the same as the sensing device except for a glass sheet placed on top in order to make the compensation device sensitive only to moisture.[47] The authors believe that the combination of data processing with an array of sensors consisting of humidity sensors would be an ideal solution.

4.3 *Effect of oxygen partial pressure*

In the working principle model of the SMO gas sensor,[48] oxygen partial pressure is also a factor that may influence the gas sensor resistance. An experiment was performed to verify this, and the result is presented in Fig. 8. After the sensor was stabilized, nitrogen at a high flow rate (2 l/min) was introduced into the test chamber (4 L). The resulting sensor

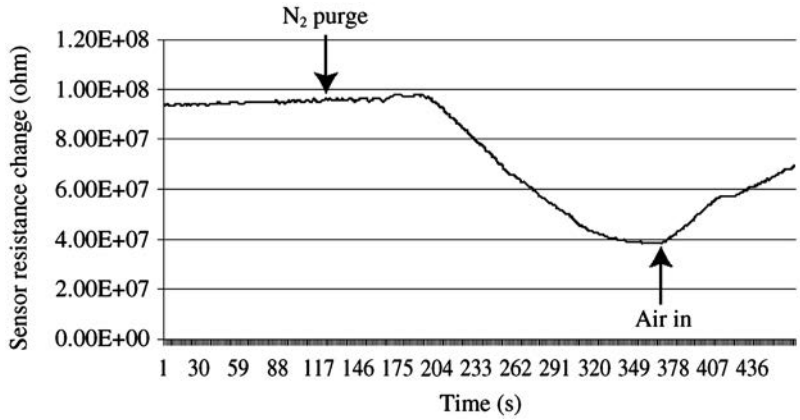

Fig. 8. Effect of oxygen partial pressure on sensor performance.

resistance did not change immediately after N_2 was introduced. However, after approximately 2 min, the resistance began to drop. Therefore, we concluded that the amount of oxygen adsorbed onto the tin oxide surface was very small and reached a saturated state even in an environment of very low oxygen concentration. However, when the oxygen partial pressure was below a critical level, further oxygen concentration changes (decreases) affected the resistance of the SMO sensor.

4.4 *Influence of light*

The authors recently evaluated the influence of light on the SMO sensor stability. This discovery and the attempt to explain this phenomenon of SMO gas sensors are presented here for the first time, to the authors' knowledge. Our preliminary test results (Fig. 9) showed that when a fluorescent lamp in the laboratory was turned off, the resistance of the gas sensor increased gradually to a certain level. When the lamp was turned on again, the sensor resistance decreased and reverted to the previous level. This test was repeated and a resistance change of approximately 20% was recorded.

The authors attributed this effect to the photoelectric phenomenon[49] that can be explained using the Bohr model. Neutrons and protons in an atom occupy a dense central region called the nucleus, and electrons orbit the nucleus. Electrons can make transitions between the orbits allowed by quantum mechanics by absorbing or emitting exactly the energy difference between the orbits. In each case, the wavelength of the emitted or absorbed light is exactly such that the photon carries the energy difference between the two orbits, i.e., hv, where h *is* Planck's constant and v *is* the frequency of the radiation. Thus, an atom can absorb or emit only certain discrete wavelengths (or equivalently, frequencies or energies). Therefore, tin dioxide absorbs a certain wavelength of light, and the acquired energy is used to emit electrons from the covalent bond to the conduction bond, thus increasing conductivity. Figure 9 shows the test result of the influence of light on the SnO_2/Ag sensor resistance when the light is on and when it is off. Ambient temperature and RH were monitored to exclude their effects on the gas sensor during the test.

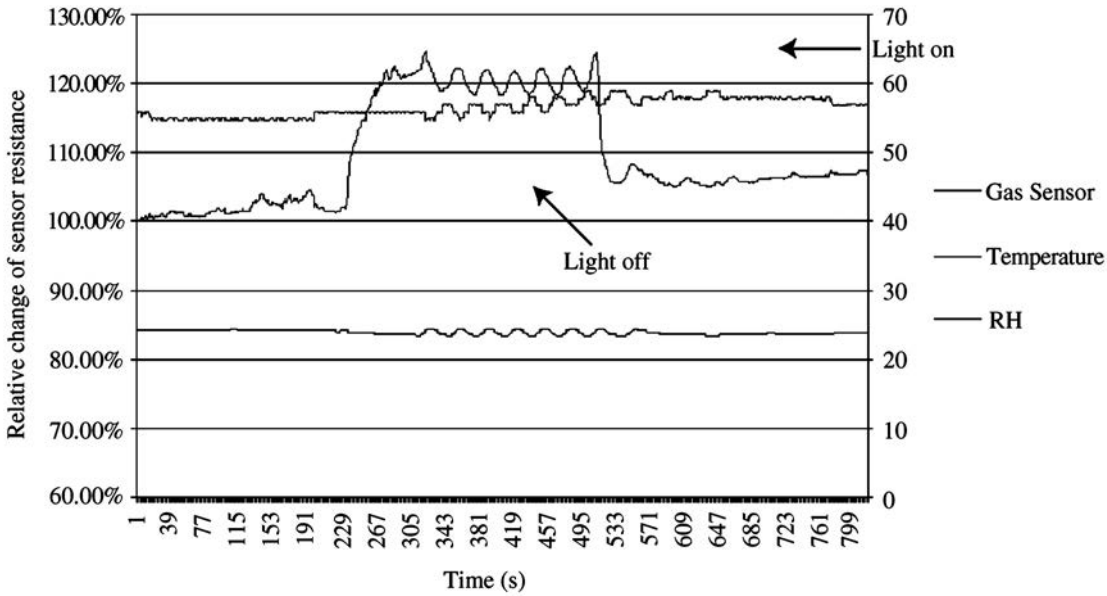

Fig. 9. Influence of light on SMO gas sensor.

5. Conclusions

Nanostructured SMO sensors fabricated by micromachining are very promising for developing the next generation of gas sensors. Their good sensing performance, in terms of good sensitivity, fast response and quick recovery, is attributed to a large surface-to-volume ratio as well as to controlled thickness and appropriate doping achieved during the sol-gel process. However, to succeed, SMO sensor development must ensure that these devices are stable under field conditions over their entire desired lifetime. Environmental factors affect the SMO sensor performance. For example, ambient temperature variations cause the sensor baseline resistance to drift. Relative humidity changes affect the baseline resistance of the SMO gas sensor and thus the sensitivity of the gas being detected. Other possible interferences include light and oxygen partial pressure. That is to say, instead of considering the resistance a constant value, the baseline resistance of a SMO gas sensor should be regarded as a function of $R = f(T, RH, v, p)$, where T is the ambient temperature, RH is the relative humidity, v is the frequency of the radiation, and p is the oxygen partial pressure. All these environmental factors cause changes in sensor baseline resistance. If they are not well accounted for, these factors will cause instability or drift of a gas sensor and most probably will cause false alarms. Although many schemes for eliminating these influences have been proposed during the development of commercial SMO gas sensors, there is still much room for improvement, both in technology and performance regarding environmentally related problems.

References

1 W. H. Brattain and J. Bardeen: Bell. Syst. Tech. J. **32** (1952) 1.
2 N. Taguchi: Japanese Patent 45-38200.
3 N. Taguchi: Japanese Patent 47-38840.
4 N. Taguchi: US Patent 3 644 795.
5 Figaro Products Catalogue (Figaro gas sensors 2000-series, Figaro Engineering Inc.).
6 FIS, Product list (May 1999, FIS Incorporated).
7 G. Blaser: Physica A **266** (1999) 218.
8 I. Simon, N. Bârsan, M. Bauer and U. Weimar: Sens. Actuators, B **73** (2001) 1.
9 N. Yamazoe: Sens. Actuators, B **5** (1991) 7.
10 H. Meixner, J. Gerblinger, U. Lampe and M. Fleischer: Sens. Actuators, B **23** (1995) 119.
11 D. E. Williams: Sens. Actuators, B **57** (1999) 1.
12 http://www.sensorsmag.com/resources/
13 B. S. Joo, N. J. Choi, Y. S. Lee, J. W. Lim, B. H. Kang and D. D. Lee: Sens. Actuators, B **77** (2001) 209.
14 I. Sayago, J. Gutiérrez, L. Arés, J. I. Robla, M. C. Horrillo, J. Rino, J. Getino and J. A. Agapito: Sens. Actuators, B **26** (1995) 19.
15 P. S. More, Y. B. Khollam, S. B. Deshpande, S. R. Sainkar, S. K. Date, R. N. Karekar and R. C. Aiyer: Mater. Lett. **57** (2003) 2177.
16 J. Gong, W. Fei, Z. Xia, Q. Chen, S. Seal and L. C. Chow: Proc. IEEE□I (2003) 124.
17 J. W. Gardner and K. C. Persaud: Handbook of Machine Olfaction: Electronic Noses and Olfaction (IOP Publishing, Bristol, 2000) 3.
18 C. Xu, J. Tamaki, N. Miura and N. Yamazoe: Sens. Actuators, B **3** (1991) 147.
19 B. Esfandyarpour, S. Mohajerzadeh, A. A. Khodadadi and M. D. Robertson: IEEE Sensors Journal **4** (2004) 449.
20 M. Ivanovskaya, P. Bogdanov, D. Orlik, A. Gurlo and V. Romanovskaya: Thin Solid Films **296** (1997) 41.
21 C. Cobianu, C. Savaniu, A. Arnautu, R. Iorgulescu, D. Dascalu, G. Leo, M. Mazzer, R. Rella, P. Siciliano, S. Capone and L. Vasanelli: Sens. Actuators, B **58** (1999) 552.
22 Y. Mo, Y. Okawa, M. Tajima, T. Nakai, N. Yoshiike and K. Natukawa: Sens. Actuators, B **79** (2001) 175.
23 S. M. Lee, D. C. Dyer and J. W. Gardner: Microelectronics Journal **34** (2003) 115.
24 A. Friedberger, P. Kreisl, E. Rose, G. Müller, G. Kühner, J. Wöllenstein and H. Böttner: Sens. Actuators, B **93** (2003) 345.
25 J. Gong, Q. Chen, W. Fei and S. Seal: Sens. Actuators, B **102** (2004) 117.
26 S. Shukla and S. Seal: Encyclopedia of Nanoscience and Nanotechnology, ed. H. S. Nalwa (American Scientific Publishers, Slevenson Ranch, CA, 2003).
27 D. W. Singh: Semiconductor Devices: Basic Principles (Wiley and Sons, New York, 2001).
28 H. Esch, G. Huyberechts, R. Mertens, G. Maes, J. Manca, W. De Ceuninck and L. De Schepper: Sens. Actuators, B **65** (200) 190.
29 http://www.figarosensor.com/
30 J. Sheng, N. Yoshida, J. Karasawa and T. Fukami: Sens. Actuators, B **41** (1997) 131.
31 http://www.investigacion.frc.utn.edu.ar/sensores/gases/gl07.pdf
32 J. Gong, Q. Chen, M. Lian, N. Liu and C. Daoust: IEEE Sensors Journal (2005) (to appear).
33 D. E. Williams and R. Catlow: Solid State Gas Sensors *(*Adam Hilger IOP Publishing, Bristol, 1987) Chap. 5.1.
34 K. Ihokura and J. Watson: The Stanic Oxide Gas Sensor (CRC Press, Boca Raton, Florida, 1994).

35 I. J. Gallardo: Tungsten Oxide Nanocrystalline Powders for Gas Sensing Applications (PhD Dissertation, University of Barcelona, Barcelona, June, 2003).
36 M. J. Madou and S. R. Morisson: Chemical Sensing and Solid State Devices (Academic Press, New York, 1989) p. 493.
37 T. Kuse and S. Takahashi: Sens. Actuators, B **67** (2000) 36.
38 R. Ionescu, A. Vancu, C. Moise and A. Tomescu: Sens. Actuators, B **61** (1999) 39.
39 I. Jiménez, J. Arbiol, G. Dezanneau, A. Cornet and J. R. Morante: Sens. Actuators, B **93** (2003) 475.
40 Z. Ling and C. Leach: Sens. Actuators, B **102** (2004) 102.
41 D. Kohl: Sens. Actuators, B **18** (1989) 71.
42 L. N. Yannopoulos: Sens. Actuators, B **12** (1987) 77.
43 N. Bârsan and R. Ionescu: Sens. Actuators, B **12** (1993) 71.
44 C. Delph, M. Siadat and M. Lumbreras: Sens. Actuators, B **59** (1999) 255.
45 P. Van Geloven, M. Honore, J. Roggen, S. Leppavuori and T. Rantala: Sens. Actuators, B **4** (1991) 185.
46 G. Huyberechts, P. Szecówka, J. Roggen and B. W. Licznerski: Sens. Actuators, B **45** (1997) 123.
47 http://www.sensorsmag.com/resources/
48 Figaro Technique Manual (1998) p. 2.
49 S. O. Kasap: Principles of Electronic Materials and Device, 2nd edition (McGraw-Hill Higher Education, Columbus, Ohio, 2002).